frontiers | Frontiers in Physics

TYPE Original Research
PUBLISHED 15 August 2023
DOI 10.3389/fphy.2023.1205650

OPEN ACCESS

EDITED BY
Eliana Maria Vasquez Osorio,
The University of Manchester,
United Kingdom

REVIEWED BY
Brígida Ferreira,
University of Lisbon, Portugal
Guillermo Cabrera-Guerrero,
Pontificia Universidad Católica de
Valparaíso, Chile

*CORRESPONDENCE
Bo Liu,
bo.liu@buaa.edu.cn
Qiuwen Wu,
qiuwen.wu@duke.edu

RECEIVED 14 April 2023
ACCEPTED 03 August 2023
PUBLISHED 15 August 2023

CITATION
Zhang X, Zhou F, Liu B, Xiong T, Bai X and Wu Q (2023), Continuous photon energy modulation in IMRT of pancreatic cancer. *Front. Phys.* 11:1205650. doi: 10.3389/fphy.2023.1205650

Continuous photon energy modulation in IMRT of pancreatic cancer

Xile Zhang[1,2], Fugen Zhou[1,3], Bo Liu[1,3]*, Tianyu Xiong[4], Xiangzhi Bai[1,3] and Qiuwen Wu[5]*

[1]Image Processing Center, Beihang University, Beijing, China, [2]Department of Radiation Oncology, Peking University Third Hospital, Beijing, China, [3]Beijing Advanced Innovation Center for Biomedical Engineering, Beihang University, Beijing, China, [4]Department of Physics, Beihang University, Beijing, China, [5]Department of Radiation Oncology, Duke University Medical Center, Durham, NC, United States

Purpose: To develop a novel IMRT optimization method based on the principle of photon energy synthesis that simultaneously optimizes fluence map and beamlet energy. The method was validated on pancreatic cancers to demonstrate the benefits of the additional degree of freedom of photon energy in IMRT.

Methods: Previous work has demonstrated that the effect of a photon beam of known energy can be achieved by the combination of two existing energy photons in the proper ratio. It further implied that any energy photon can be synthesized. Based on this, we propose the concept of continuous beamlet energy modulation in IMRT, or IMRT-BEM. The IMRT-BEM was modeled as the simultaneous optimization of two fluence maps, one for the low energy beam and one for the high energy beam, and it was implemented in an in-house inverse planning system. The IMRT-BEM was applied on 10 pancreatic cancer cases, where the IMRT-BEM plan was compared with single-energy IMRT plans of 6 MV (IMRT-6MV) and 15 MV photons (IMRT-15MV).

Results: The IMRT-BEM plan provides a noticeable reduction to the volume irradiated at the high dose level ($PTV_{105\%}$) for PTV, at least 24.7% (6.4 $\pm$ 6.8 vs. 31.1 $\pm$ 18.7 (p = 0.005) and 43.8 $\pm$ 19.8 (p = 0.005) for IMRT-BEM, IMRT-6MV, and IMRT-15MV respectively). For target dose coverage, there were statistically significant improvements between the IMRT-BEM plans and the other two plans in terms of CI and HI. Compared to the IMRT-6MV plan, there were significant reductions in the D_{mean} of the spinal cord, liver, bowel, duodenum, and stomach. The irradiation volumes of the medium dose (V_{20Gy}, and V_{40Gy}) for the duodenum and bowel were reduced significantly. There were no significant differences between the IMRT-BEM and IMRT-15MV plans except for the D_{mean} of the spinal cord and the duodenum, the V_{20Gy}, and V_{40Gy} for the duodenum, and the V_{20Gy} of the stomach.

Conclusion: IMRT-BEM has certain dosimetric advantages for PTV and improves OAR sparing in pancreatic cancer, and can be effectively used in radiation treatment planning, providing another degree of freedom for planners to improve treatment plan quality.

KEYWORDS

photon energy synthesis, continuous photon energy modulation, intensity-modulated radiation therapy, IMRT optimization, pancreatic cancer

1 Introduction

Intensity-modulated radiation therapy (IMRT) was introduced about four decades ago [1] and has proven to produce superior dose distributions to 3D conformal techniques for almost all anatomic sites, particularly those with concave targets [2]. IMRT can deliver tightly conformal dose distributions and have better sparing to organs at risk (OAR) through the generation and realization of non-uniform fluence maps across multiple radiation beams. There is a wide range of literature on IMRT optimization [3–7]. The process of IMRT optimization, as a multi-criteria problem, needs to define an objective function to quantitatively evaluate the deviation between the planned dose and the target dose, including the dose constraints for both target and OARs [8]. To solve the problem, the IMRT optimization process is traditionally classified into two categories: 1) "two-step method": optimizing the photon fluence map in each field (fluence map optimization, FMO) and then generating sub-field leaf sequences sequentially [9, 10]; 2) direct aperture optimization (DAO): directly optimizing leaf sequences to obtain desired dose distribution [11, 12].

A modern Linac is often equipped with multiple photon energies (usually two photon energies) [13]. The clinically relevant energy range for photons was 6–18 MV. It was known that the physical deposition capability in the medium is energy dependent. Generally, lower energy photon beams (≤6 MV) have limited penetration and are often used to treat superficial or shallow tumors. Due to the benefit of narrow penumbra, the IMRT plan using lower energy photon generated a tighter dose distribution around the target and better preserves the critical structures adjacent to the target volume. However, it results in a higher entrance dose [14]. On the other hand, higher energy photon beams (≥10 MV) are often used to treat deep-seated tumors, such as prostate or gynecological tumors et al, for their higher penetration and better skin-sparing ability. However, the resulting neutron contamination and higher exit dose should be of concern in clinical practice [14].

One challenge in IMRT is the selection of beam energy in traditional treatment planning, which requires the consideration of the overall characteristics of the clinical case. The energy of photon is closely related to the depth of the tumor or the size of the patient. For deep tumor and large size patient, the high energy photon has advantages over the low-energy photon [15]. However, the involvement of many OARs nearby with different dose tolerances and the use of multiple cross-firing beams often makes the selection of optimal energy not obvious. The optimal energy is usually decided on a trial-and-error basis [16], based on the tumor location and clinical experience. Previous papers have shown some energy dependence for different treatment modalities and tumor sites [17–19]. There was a dose increment in regions distant from the target volume when 6 MV photon was used instead of 10 or 18 MV photons in an IMRT plan with less than nine fields [15]. When a sufficient number of fields were used, such dose increment becomes less and the plan quality is no longer sensitive to beam energy, even for exceptionally large patients [15]. However, these observations are only applicable to plans with a single energy.

Recently, some studies have shown the potential dosimetric gains of mixed energy photons (one low-energy and one high-energy photon) [20–23]. In these works, the beam energy is generally assigned based on the one-dimensional effective path length (EPL) of tumor depth. The general findings are that the mixed-energy photon plan has advantages in terms of increasing dose coverage and conformity to PTV, or sparing relevant OARs, but the advantages are not significant. However, these studies simply used two energies available from a Linac and did not fully demonstrate the dose deposition characteristics of different energies. Some works incorporate photon energy as a parameter in the plan optimization. St-Hilaire et al introduced an energy angle concept as an additional, independent degree of freedom for multiple-energy optimization (MEO) using DAO [24]. McGeachy et al provided the algorithm for simultaneously optimizing both beamlet energy and fluence in IMRT and found potential dosimetric benefits in OARs sparing [25]. All these attempts proved that the extra degree of freedom of photon energy can bring some dosimetric gains, and improve the overall plan quality. However, the optimization is more demanding in terms of computation and memory, due to the significantly increased number of variables [24]. Currently, all these studies only selected two energy photons for optimization. If more levels of energy are introduced to the IMRT optimization, the computational complexity and time requirements would increase significantly, which makes the IMRT optimization impracticable [24].

In our previous works [26, 27], it was shown that any intermediate energy photon can be effectively synthesized from a combination of two different energy photons. This technique also enables continuous energy modulation in IMRT, providing another degree of freedom to improve treatment plan quality. Therefore, the purpose of this study was to develop and validate a novel IMRT method that can simultaneously optimize fluence map and beamlet energy, referred to as IMRT with beamlet energy modulated (IMRT-BEM). Based on the energy synthesis principle, the IMRT-BEM was modeled as the optimization of two fluence maps for one low energy and one high energy photon beams, and it was implemented in an in-house inverse planning system. Since the principle showed that any energy photon can be synthesized using two energy photons, it implies that no more than two energy photons are necessary from the same gantry angle. This is fundamentally different from previous studies of trial-and-error that are based on the belief of "more is better". The IMRT-BEM was analyzed and demonstrated on ten pancreatic cancer cases. To investigate the impact of incorporating an additional degree of freedom in beamlet energy, the dose distributions resulting from IMRT-BEM plans were compared to conventional single energy IMRT plans utilizing either 6 MV beams (IMRT-6MV) or 15 MV beams (IMRT-15MV). To the best of our knowledge, there are no previous works on multi-energy IMRT optimization that validated the method in a large number of clinical cases.

2 Materials and methods

2.1 Continuous energy synthesis strategy

Previous research has demonstrated that a photon beam of known energy can be synthesized by combining two existing energy photons from a medical linear accelerator even under the most stringent criteria [27]. This technology also implies that, according to the formulation 1), the beam characteristics of any continuously

adjustable synthetic photon energy (E_{syn}) can be synthesized with variable weighting coefficients (α, β) for one low energy (E_{low}) and one high energy (E_{high}) photons.

$$\begin{cases} \boldsymbol{pdd}\left(E_{syn}\right) = \alpha \cdot \boldsymbol{pdd}\left(E_{low}\right) + \beta \cdot \boldsymbol{pdd}\left(E_{high}\right), \\ \boldsymbol{ocr}\left(E_{syn}\right) = \alpha \cdot \boldsymbol{ocr}\left(E_{low}\right) + \beta \cdot \boldsymbol{ocr}\left(E_{high}\right), \end{cases} \tag{1}$$

where ***pdd*** is the percent depth dose (PDD), and ***ocr*** is the off-center ratio (OCR). The subscript indicates the corresponding energy.

Thus, a linear accelerator equipped with 6 MV and 15 MV photon energies could be operated according to this method to yield any energy in-between, e.g., 6, 7, 8, 9, 10, 11, 12, 13, 14, 15 MV photons, and even a non-integer energy photon. In other words, we can synthesize photons with any continuous energy between 6 and 15 MV. Generally, the larger the β value, the larger the proportion of the high-energy part and the synthesized energy E_{syn} are higher. It should be noted that the object of this study is photon beam, not electron beam, and the unit of beam energy mentioned here is MV (not MeV).

2.2 Single-energy optimization algorithm

The relationship between dose and fluence in FMO was formulated by the following Eq. 2

$$\boldsymbol{d} = \boldsymbol{A} \cdot \boldsymbol{x}, \tag{2}$$

where $\boldsymbol{d}$ is a $m \times 1$ voxel dose vector, $\boldsymbol{x}$ is the $n \times 1$ beamlet fluence vector, and $\boldsymbol{A}$ is the precalculated dose deposition matrix with a dimension of $m \times n$. For IMRT, the number of voxels generally is about 10^5, and the number of beamlets is about 10^4 [28].

Generally, in IMRT treatment planning, a certain number of beams with different gantry angles are initially selected according to the positions of the tumor and the OARs. Then only a single suitable energy is usually selected for all beams. Afterward, optimization objectives are set to construct a mathematical optimization problem and the plan parameters are obtained by solving this problem. Commonly, a weighted sum of objectives is optimized to obtain the solution $\boldsymbol{x}$ which also must satisfy certain constraints, i.e., the resulting plan must be clinically acceptable. The optimization objective f_i is based on a function of dose, dose volume, or equivalent uniform dose (EUD). Therefore, the inverse optimization problem has the following form of objective function:

$$min \sum_{i=1}^{N} \omega_i \cdot f_i(\boldsymbol{D}), \tag{3}$$

where $\boldsymbol{D}$ is the dose distribution of the target and OARs, considered as a function of $\boldsymbol{x}$. ω_i is the penalty factor, selected according to the clinical importance of the target and OARs.

2.3 IMRT with beamlet energy modulated

To model the IMRT-BEM, the relationship of dose and fluence was reformatted to the following Eq. 4:

$$\boldsymbol{d} = \sum_{j=1}^{n} \boldsymbol{A}_j \cdot \boldsymbol{x}_j, \tag{4}$$

where j indexes the jth-beamlet; $\boldsymbol{A}_j$ is the dose deposition vector for the jth-beamlet; $\boldsymbol{x}_j$ is the jth-beamlet fluence. Based on the expression 1), we constructed the jth-beamlet energy deposition vector $\boldsymbol{A}_j$ as follows:

$$\boldsymbol{A}_j = \alpha_j \cdot \boldsymbol{A}_j^{E_{low}} + \beta_j \cdot \boldsymbol{A}_j^{E_{high}}, \tag{5}$$

where $\boldsymbol{A}_j^{E_{low}}$ and $\boldsymbol{A}_j^{E_{high}}$ are the dose deposition vector for the jth-beamlet with E_{low} and E_{high}; α_j and β_j. Are the energy synthesis weighting coefficients.

Then Eq. 4 can be replaced by Eq. 6 with additional variables of the weighting coefficients matrices (α_j, β_j).

$$\boldsymbol{d} = \sum_{j=1}^{n} \alpha_j \cdot \boldsymbol{A}_j^{E_{low}} \cdot \boldsymbol{x}_j + \sum_{j=1}^{n} \beta_j \cdot \boldsymbol{A}_j^{E_{high}} \cdot \boldsymbol{x}_j, \tag{6}$$

By defining $\boldsymbol{y}_j^{E_{low}} = \alpha_j \cdot \boldsymbol{x}_j$ and $\boldsymbol{y}_j^{E_{high}} = \beta_j \cdot \boldsymbol{x}_j$, we get the following formula from Eq. 6:

$$\begin{aligned} \boldsymbol{d} &= \sum_{j=1}^{n} \boldsymbol{A}_j^{E_{low}} \cdot \boldsymbol{y}_j^{E_{low}} + \sum_{j=1}^{n} \boldsymbol{A}_j^{E_{high}} \cdot \boldsymbol{y}_j^{E_{high}} \\ &= \boldsymbol{A}^{E_{low}} \cdot \boldsymbol{y}^{E_{low}} + \boldsymbol{A}^{E_{high}} \cdot \boldsymbol{y}^{E_{high}}. \end{aligned} \tag{7}$$

Based on the relationship provided in Eqs 6, 7, we can achieve the simultaneous optimization of the fluence intensity and the beamlet energy by only optimizing high-energy and low-energy fluence maps ($y_j^{E_{low}}$ and $y_j^{E_{high}}$) for each beam. The ratio of $y_j^{E_{low}}$ and $y_j^{E_{high}}$ determines the optimal photon energy for the jth-beamlet. The resulting dose in each voxel is a linear combination of the dose contributions from photons with energies E_{low} and E_{high}. Therefore, this strategy offers the opportunity to use continuous beamlet energy modulation in IMRT. The number of beamlets is merely doubled, and compared with other energy optimization methods, this approach does not introduce much complexity to IMRT optimization.

After fluence optimization, the optimized fluence distribution for each energy was converted into a sequence of MLC shapes with corresponding weights (MUs). Finally, the IMRT-BEM plan can be delivered with two single-energy photon plans at E_{low} and E_{high}, respectively.

2.4 Patient data and plan optimization

Pancreatic cancer cells are relatively resistant to radiation, so higher radiation doses are often required for the target volume. However, the dose-limiting OARs such as the stomach, bowel, and duodenum close to the pancreas are inevitably irradiated, resulting in complications such as nausea, vomiting, gastrointestinal bleeding, and irreversible hepatic or renal impairment [29]. It is particularly important to protect the OARs to the greatest extent while ensuring high-dose irradiation in the target volume. Among these organs at risk, there are both serial and parallel organs, each with different volumes and distances to the target. Therefore, these OAR dose constraints may affect dose coverage and homogeneity of the target in IMRT optimization. We know that different energy photon beams have different penetration capabilities and other dosimetric properties, so IMRT-BEM may have some dosimetric advantages in IMRT optimization for pancreatic cancer.

Ten patients with pancreatic cancer were included. The planning CT was acquired with a slice thickness of 3 mm. Target volumes

TABLE 1 Template of dose-volume constraints and weighting factors in IMRT optimization for the pancreatic cancer cases.

Structure	Constraint	Value	Weighting factor
PTV	Min Dose	55 Gy	230
	Max Dose	56 Gy	200
Kidneys	Max DVH V_{15Gy}	20%	100
Liver	Max DVH V_{20Gy}	20%	100
Spinal Cord	Max Dose	40 Gy	100
Stomach	Max Dose	52 Gy	150
	Max DVH V_{20Gy}	40%	100
	Max DVH V_{40Gy}	20%	100
Duodenum	Max Dose	52 Gy	150
	Max DVH V_{20Gy}	40%	100
	Max DVH V_{40Gy}	20%	100
Bowel	Max Dose	52 Gy	150
	Max DVH V_{20Gy}	40%	100
	Max DVH V_{40Gy}	20%	100
Ring1	Max Dose	43.2 Gy	50
Ring2	Max Dose	37.8 Gy	50
Ring3	Max Dose	32.4 Gy	50

including GTV, CTV, and PTV were delineated by a radiation oncologist. The OARs including the liver, bowel, spinal cord, kidneys, duodenum, and stomach were contoured [30]. The normal tissue was defined as the tissues inside of the body contour excluding PTV [31].

For all ten cases, three plans of IMRT-6MV, IMRT-15MV, and IMRT-BEM were generated and compared to evaluate the effect of energy modulation in the IMRT optimization. Each plan used the same 5 non-equidistance co-planar fields with gantry angles of 0°, 60°, 150°, 210°, and 300°, respectively. The plan was optimized using a quadratic objective in an in-house IMRT treatment planning system (TPS), and the dose was calculated using the collapsed cone algorithm. The TPS used the beam data of the Varian TrueBeam unit with two photon energies of 6 MV and 15 MV.

The prescription dose was 54 Gy to the PTV in 27 fractions. The goals for PTV were a minimum dose of at least 95% and a maximum dose of 105% of the prescription dose for PTV. According to our institutional protocol based on relevant literature [32], OARs dose constraints included the following: $V_{30Gy} < 30\%$ and $D_{mean} < 20$ Gy for the liver; $D_{max} < 52$ Gy and $V_{45Gy} < 15\%$ for the bowel, the duodenum, and the stomach; $D_{max} < 45$ Gy for the spinal cord; $V_{18Gy} < 30\%$ for the kidneys. The constraint template for the dose volume of the PTV, OARs, and ring structures in IMRT optimization is provided in Table 1. It should be noted that the dose constraints and optimization weights will be appropriately adjusted to achieve individual optimization. But for each patient, the dose constraints and optimization weights were kept the same for all plans. Therefore, the results of plan quality mainly reflected the physical beam characteristics of different energy.

2.5 Plan evaluation

All plans were normalized that 100% of the prescription dose isodose line covered 95% of the PTV volume. Quantitative analysis was performed to compare the relevant dosimetric indices of the IMRT-BEM plans with the other two solutions. The ICRU 83 report was used as the protocol for plan evaluation in this study [33]. For target evaluation, the mean dose (D_{mean}), the minimum doses delivered to 2%, 98%, and 50% of PTV ($D_{2\%}$, $D_{50\%}$, and $D_{98\%}$), and the volumes of PTV covered by the 95% and 105% of the prescription dose ($PTV_{95\%}$ and $PTV_{105\%}$) were compared. The homogeneity index (HI) (HI = 0, for a perfectly homogenous dose distribution) and conformity index (CI) (CI = 1, for a perfect coverage dose distribution) were used for the PTV dose distribution evaluation [33].

Some selected DVH dosimetric indices of OARs were analyzed, including the mean doses (D_{mean}), V_{15Gy}, and V_{30Gy} of the kidneys and the liver, D_{max}, D_{mean}, V_{20Gy}, and V_{40Gy} of the stomach, bowel, and duodenum. Additionally, a comparison was made for Dmax and Dmean of the spinal cord. For normal tissue, the integral dose was compared, which was defined as the volume of structure multiplied by the mean dose to the normal tissue [31].

Plans were also evaluated by comparing the objective function values, the number of monitor units (MUs), the dose-volume histograms (DVHs), and the isodose distributions for each plan. The fluence map distributions of each beam at energies E_{low} and E_{high} were also analyzed.

To investigate the effect of the number of fields on the energy dependence of the plan [15], additional plans were generated with a range of number of beams (3–11), and the objective function values were compared.

Statistical analysis was performed via the Wilcoxon rank-sum test in SPSS 24.0 software (SPSSInc., Chicago, Ill., United States) to analyze the differences in planned dose distribution between IMRT-BEM and the other two solutions. A p-value less than 0.05 was considered statistically significant.

3 Results

3.1 DVHs and isodose distributions

Benefiting from the distinct penetration capabilities and other dosimetric properties of different energy photons, IMRT-BEM plans could produce a more homogenous dose to the target volume, a tighter dose distribution around the target, and spare more of the adjacent critical structures. As an illustrative example, Figure 1 displays the 56.7, 54.0, 50.0, 40.0, 30.0, 20.0, and 10.0 Gy isodose lines for the optimized plans in axial, coronal, and sagittal planes. IMRT-BEM plan is more conformal in comparison to IMRT-6MV and IMRT-15MV plans in the axial plane (indicated by the red arrow). In addition, the 30 and 40 Gy isodose lines (indicated by the yellow arrow) covered less volume in IMRT-BEM. The high-dose irradiation volume ($PTV_{105\%}$, indicated by the purple arrow) in the PTV of IMRT-BEM was smaller than other plans in the coronal and sagittal planes. Figure 2 shows the DVH lines of the IMRT-BEM and other plans for the same patient. The PTV line of IMRT-BEM was steeper than other plans. Some OARs such as duodenum and liver,

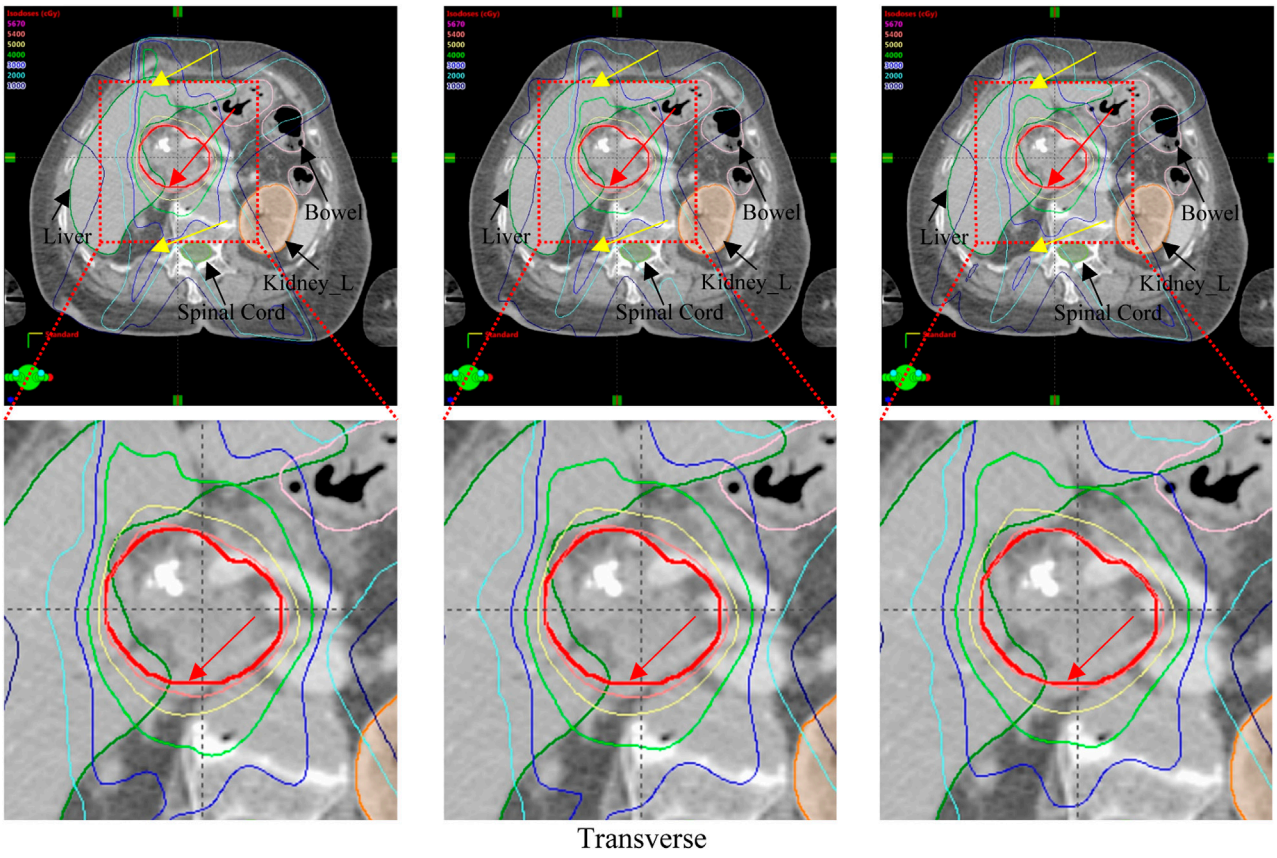

FIGURE 1
(Continued).

were slightly superior in sparing to other plans (IMRT-6MV or IMRT-15MV).

3.2 Objective function value and MU evaluation

The objective function values and the MUs for the final plans are presented in Figures 3, 4.

Figure 3 shows that, for each case, the IMRT-BEM plans achieved the lowest objective function values (p = 0.005, and 0.005 for IMRT-6MV, and IMRT-15MV, respectively). There was no obvious difference in objective function values between IMRT-6MV and IMRT-15MV plans (p = 0.139).

Figure 4 compared the MUs of IMRT-6MV, IMRT-15MV, and IMRT-BEM plans after converting the fluence map into dynamic MLC leaf sequences. The labels "IMRT-BEM:6 MV" and "IMRT-BEM:15 MV" indicate the respective contributions of 6 MV and 15 MV photons to the total MUs of the IMRT-BEM plan. For each case, the total MU for the IMRT-15MV plan was the lowest, and the IMRT-BEM plan was the highest. The IMRT-BEM plan provided an average MUs increase of 27% (than IMRT-6MV plan), and 36% (than IMRT-15MV plan). The ratio of 6 MV MUs contributions to the total number of MUs varied little in IMRT-BEM plans, ranging from 0.49 to 0.54.

3.3 Dosimetric results of PTV

The volumes of PTV range from 49 cm^3 to 143 cm^3. Overall, all plans achieved that 98% of PTV was covered by 95% of the prescription dose. Additional PTV dosimetric results for each patient are presented in the Supplementary Material.

Table 2 summarized the dosimetric comparison of PTV for all patients. It can be seen that the dosimetric parameters of the PTV of IMRT-BEM plans were significantly superior to the other two solutions. The IMRT-BEM plans provided a noticeable reduction to the volume irradiated at the high dose level ($PTV_{105\%}$) for PTV, at least 24.7% (6.4 ± 6.8 vs. 31.1 ± 18.7, and 43.8 ± 19.8, for IMRT-BEM, IMRT-6MV, and IMRT-15MV, respectively. p = 0.005, and 0.005). The $D_{2\%}$, $D_{98\%}$, $D_{50\%}$, and D_{mean} of the PTV were significantly reduced compared with the other two solutions. For target dose coverage, there were statistical improvements in terms of CI and HI.

3.4 Dosimetric results of OARs and normal tissue

The essential dosimetric results of OARs are shown in Table 3. Additional dosimetric results for OARs can also be found in the Supplementary Material. Comparing IMRT-BEM to the IMRT-

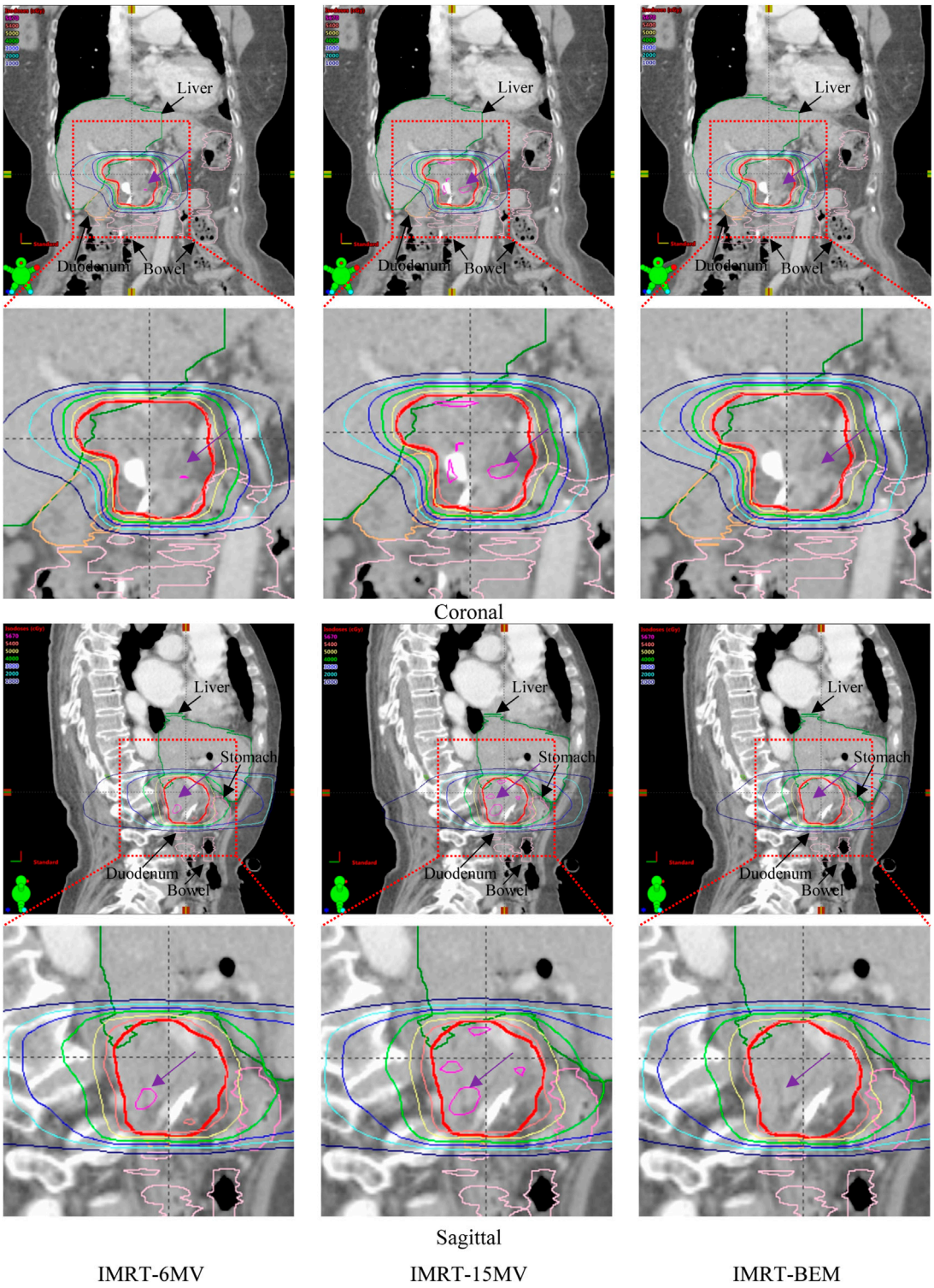

FIGURE 1
(Continued). Comparison of isodose distributions of IMRT plans for one case (The thick red solid lines represent PTV). The red arrows indicate a tighter dose distribution with better avoidance of OARs in IMRT-BEM plans. The yellow arrows indicate the 30 and 40 Gy isodose lines covered less volume in IMRT-BEM. The purple arrows indicate high-dose irradiation volume ($PTV_{105\%}$) in the PTV of IMRT-BEM was less than other plans in the coronal and sagittal planes.

6MV plans, there was a statistically significant reduction in the D_{mean} of the spinal cord, liver, bowel, duodenum, and stomach. The mean volumes of the medium dose for the duodenum (V_{20Gy} and V_{40Gy}) were reduced by 2.5% and 0.6%, respectively. The V_{20Gy} and V_{40Gy} of the bowel were reduced by 0.8% and 0.2%, respectively. The V_{20Gy} of the stomach was reduced by 1.1%.

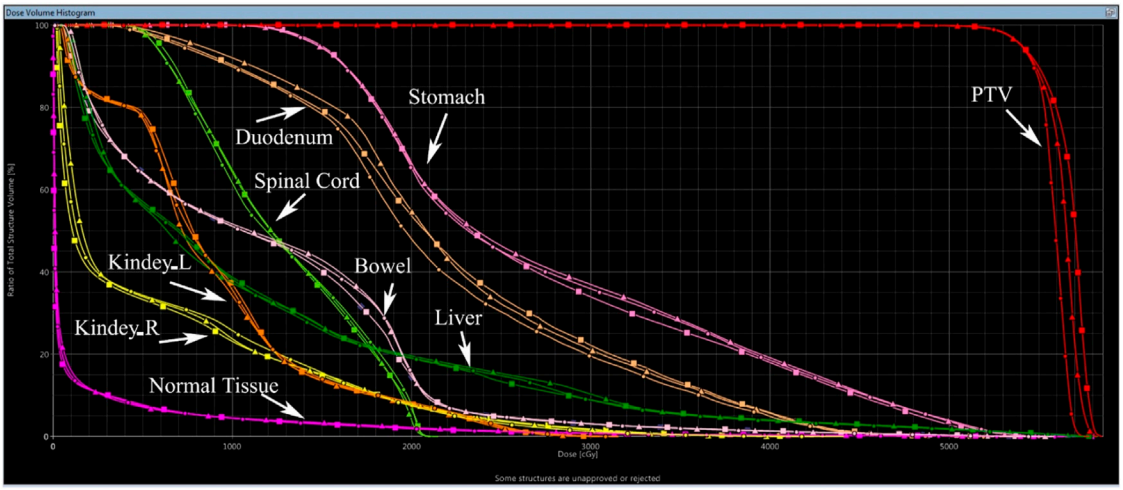

FIGURE 2
Dose-volume histograms of IMRT plans for one case. (Square solid line: IMRT-15MV; triangle solid line: IMRT-6MV; dot solid line: IMRT-BEM).

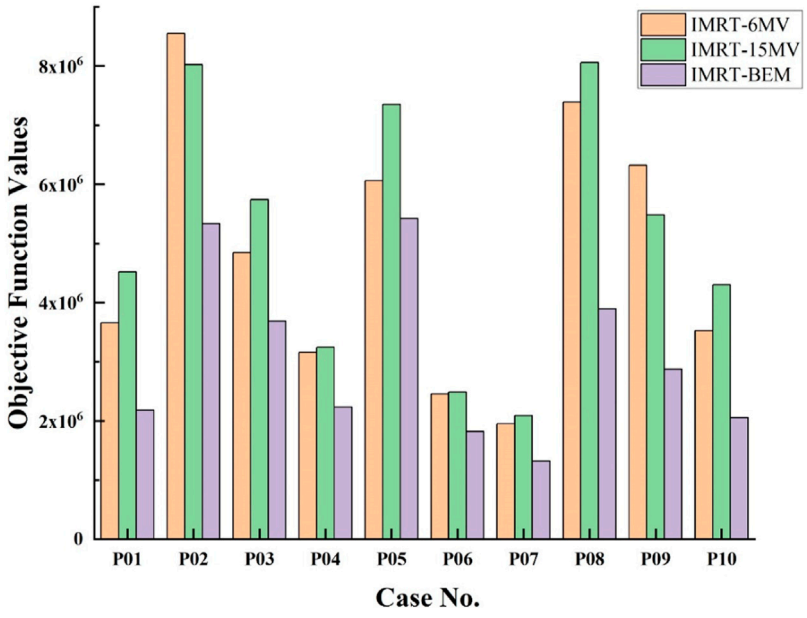

FIGURE 3
Comparison of values of the objective function of IMRT-6MV, IMRT-15MV, and IMRT-BEM plans for the 10 cases.

There were no significant differences in most of the dosimetric parameters between the IMRT-BEM and IMRT-15MV plans, except for the D_{mean} of the spinal cord and duodenum, the V_{20Gy} and V_{40Gy} of the duodenum by about 2.6% and 0.4%, and V_{20Gy} of the stomach by about 0.8%, respectively.

IMRT-BEM plan produced a lower non-target tissue integral dose compared to the IMRT-6MV plan (64.41 ± 17.6 vs. 61.6 ± 16.7, p = 0.008), but a slightly larger value than the IMRT-15MV plan with statistically significant (60.1 ± 16.3 vs. 61.6 ± 16.7, p = 0.007), as shown in Table 3.

3.5 The fluence map distribution

Each beam of the optimized IMRT-BEM plan was composed of beamlets with different photon energies. According to the theory of continuous photon energy synthesis described in Section 2.1, the composite fluence map of each beam was composed of the fluence maps of two energy (E_{low} and E_{high}) photons. Taking a case as an example, Figure 5 showed fluence map distributions of five fields for the IMRT-BEM plan in one case.

As shown in Figure 5, each pixel value represents the fluence of a beamlet with the energy E_{syn}.While E_{syn} is unknown, it falls in

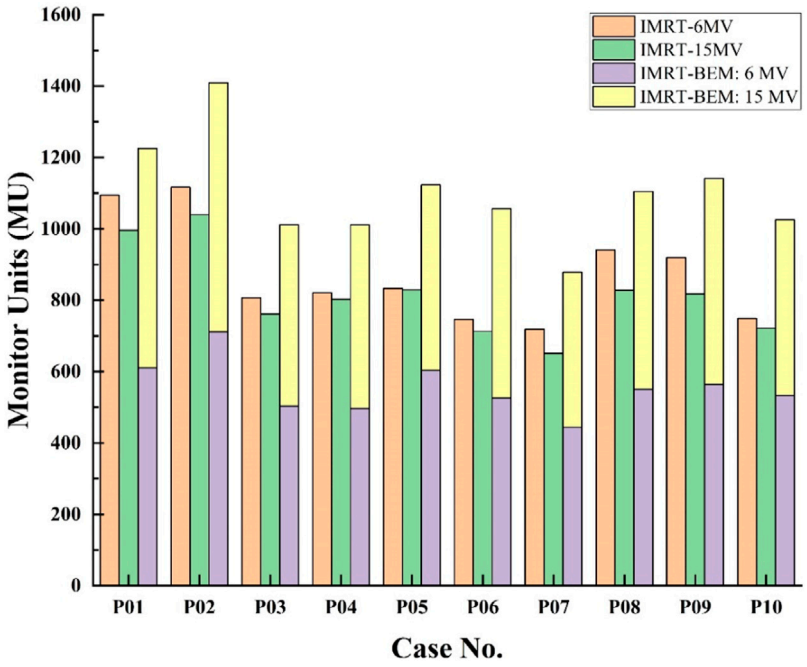

FIGURE 4
Comparison of the MUs of IMRT-6MV, IMRT-15MV, and IMRT-BEM plans for the 10 cases.

TABLE 2 Comparison of PTV dosimetric indices between IMRT-BEM and single-energy IMRT for the 10 cases.

Dosimetric parameter	IMRT-6MV (Avg. ±STD)	IMRT-15MV (Avg. ±STD)	IMRT-BEM (Avg. ±STD)	*p*-value	
				IMRT-6MV vs. IMRT-BEM	IMRT-15MV vs. IMRT-BEM
$D_{2\%}$ (Gy)	57.6 ± 0.6	57.8 ± 0.5	56.7 ± 0.5	0.005	0.005
$D_{98\%}$ (Gy)	52.9 ± 0.2	52.9 ± 0.2	53.1 ± 0.2	0.005	0.008
$D_{50\%}$ (Gy)	56.3 ± 0.4	56.6 ± 0.4	55.6 ± 0.3	0.005	0.005
D_{mean} (Gy)	56.1 ± 0.4	56.4 ± 0.4	55.5 ± 0.3	0.005	0.005
$PTV_{95\%}$ (%)	99.5 ± 0.2	99.4 ± 0.3	99.6 ± 0.2	0.007	0.005
$PTV_{105\%}$ (%)	31.1 ± 18.7	43.8 ± 19.8	6.4 ± 6.8	0.005	0.005
CI	0.82 ± 0.04	0.82 ± 0.02	0.84 ± 0.03	0.007	0.005
HI	0.08 ± 0.01	0.09 ± 0.01	0.07 ± 0.01	0.005	0.005

between E_{low} and E_{high}. The high energy (15 MV) fluence distributions were mainly in the central area of the beam field, and the low energy (6 MV) fluence distributions were mainly at the edge of the beam field or some areas overlapping with the projection of OARs. The fluence distribution was consistent with the intuition in selecting photon energy for a beam in treatment planning. A high energy photon with higher penetration is required for the interior of the tumor volume. While, in the periphery of the tumor, to obtain better conformity to the target, or to protect the OARs close to the target, a low energy photon with lower penetration should be considered as the initial option.

3.6 The effect of the number of fields

For the 10 cases, three different plans (IMRT-6MV, IMRT-15MV, and IMRT-BEM) were generated using 3, 5, 7, 9, and 11 equidistant coplanar beams, respectively. The values of the objective function were used to evaluate the plan quality, and the results are shown in Figure 6. The IMRT-BEM plans achieved the lowest objective function values when the number of beams is less than 9. When the number of beams increased, the energy dependence gradually decreases, and the objective function values of different plans are close to the same.

TABLE 3 Comparison of OAR dosimetric indices between IMRT-BEM and single-energy IMRT for the 10 cases.

Dosimetric parameter		IMRT-6MV (Avg. ± STD)	IMRT-15MV (Avg. ± STD)	IMRT-BEM (Avg. ± STD)	*p*-value	
					IMRT-6MV vs. IMRT-BEM	IMRT-15MV vs. IMRT-BEM
Spinal Cord	D_{mean} (Gy)	8.2 ± 3.6	8.0 ± 3.5	7.9 ± 3.5	**0.005**	**0.038**
	D_{max} (Gy)	28.7 ± 5.4	28.9 ± 5.2	29.0 ± 5.4	0.285	0.646
Liver	V_{15Gy} (%)	6.1 ± 8.5	6.2 ± 8.5	6.0 ± 8.3	0.398	0.128
	V_{30Gy} (%)	2.0 ± 3.2	1.9 ± 2.8	1.8 ± 2.8	0.115	0.752
	D_{mean} (Gy)	3.7 ± 3.3	3.6 ± 3.4	3.6 ± 3.3	**0.021**	0.476
Bowel	V_{20Gy} (%)	14.5 ± 6.6	13.5 ± 6.4	13.7 ± 6.1	**0.025**	0.508
	V_{40Gy} (%)	1.9 ± 1.5	1.6 ± 1.2	1.7 ± 1.3	**0.028**	0.066
	D_{mean} (Gy)	9.8 ± 2.6	9.6 ± 2.6	9.6 ± 2.4	**0.047**	0.878
	D_{max} (Gy)	54.7 ± 4.9	54.5 ± 5.4	54.3 ± 4.2	0.241	0.241
Right Kidney	V_{15Gy} (%)	10.0 ± 5.0	9.8 ± 5.4	9.5 ± 5.2	0.374	0.953
	V_{30Gy} (%)	0.8 ± 1.4	0.6 ± 0.8	0.7 ± 1.0	0.345	0.345
	D_{mean} (Gy)	6.7 ± 2.3	6.6 ± 2.4	6.7 ± 2.4	0.878	0.878
Left Kidney	V_{15Gy} (%)	7.7 ± 4.9	7.8 ± 5.2	8.0 ± 5.2	0.508	0.575
	V_{30Gy} (%)	0.7 ± 1.4	0.5 ± 1.2	0.6 ± 1.1	0.400	0.173
	D_{mean} (Gy)	6.6 ± 2.1	6.6 ± 2.2	6.6 ± 2.2	0.767	0.878
Duodenum	V_{20Gy} (%)	38.6 ± 17.5	38.7 ± 18.6	36.1 ± 17.5	**0.007**	**0.007**
	V_{40Gy} (%)	6.4 ± 3.7	6.2 ± 3.7	5.8 ± 3.4	**0.005**	**0.005**
	D_{mean} (Gy)	18.1 ± 5.4	17.9 ± 5.3	17.5 ± 5.2	**0.009**	**0.007**
	D_{max} (Gy)	52.6 ± 0.8	52.6 ± 1.1	52.8 ± 0.8	0.241	0.241
Stomach	V_{20Gy} (%)	18.4 ± 20.1	18.1 ± 19.9	17.3 ± 19.3	**0.008**	**0.038**
	V_{40Gy} (%)	3.6 ± 5.8	3.3 ± 5.4	3.4 ± 5.6	0.161	0.176
	D_{mean} (Gy)	9.4 ± 7.8	9.1 ± 7.8	9.1 ± 7.7	**0.009**	0.332
	D_{max} (Gy)	45.5 ± 17.0	44.7 ± 17.3	45.3 ± 16.8	0.799	0.445
Non-target Tissue	Integral Dose (Gy-L)	64.1 ± 17.6	60.1 ± 16.3	61.6 ± 16.7	**0.008**	**0.007**

4 Discussion

In this work, a new IMRT optimization algorithm for continuous photon beamlet energy modulation was developed and demonstrated in 10 pancreatic cancer cases, to show the effect of an additional degree of freedom of beamlet energy on plan quality. IMRT-BEM simultaneously optimizes the photon fluence and energy in each beamlet, which is theoretically different from the traditional single-energy IMRT optimization method. In contrast to the traditional IMRT optimization, where the photon energy was fixed at a pre-selected value, the photon energy of each beamlet in the IMRT-BEM plan could continuously vary within the range of min 6)—max (15) MV, and the photon energy of the beamlet is a free variable in optimization.

It is widely recognized that high-energy photon beams with energies of 10 MV or higher are commonly used in radiation therapy for deep-seated tumors. They offer excellent penetration power and protect the skin during treatment. However, it should be noted that these high-energy beams may lead to an increase in the range of secondary electrons, which can result in greater lateral scattering [34]. This can cause blurring of dose boundaries and potentially inadequate delivery of the required dose to the target area. Additionally, there is a concern regarding neutron contamination [35]. In light of these challenges, there has been a growing interest in exploring the potential dosimetric advantages of lower energy photons, such as, Cobalt-60 and low-energy X-rays (<6 MV). By utilizing lower energy photons, it may be possible to mitigate some of the issues associated with high-energy beams. Lower energy photons exhibit reduced secondary electron ranges, which can result in sharper dose boundaries and improved delivery of the desired dose to the target area. One notable advantage of low-energy photon beams is their ability to create a smaller penumbra, resulting in a more precise and tightly-focused dose distribution around the target volume [36]. Furthermore, the use of lower energy photons can potentially address concerns related to neutron contamination.

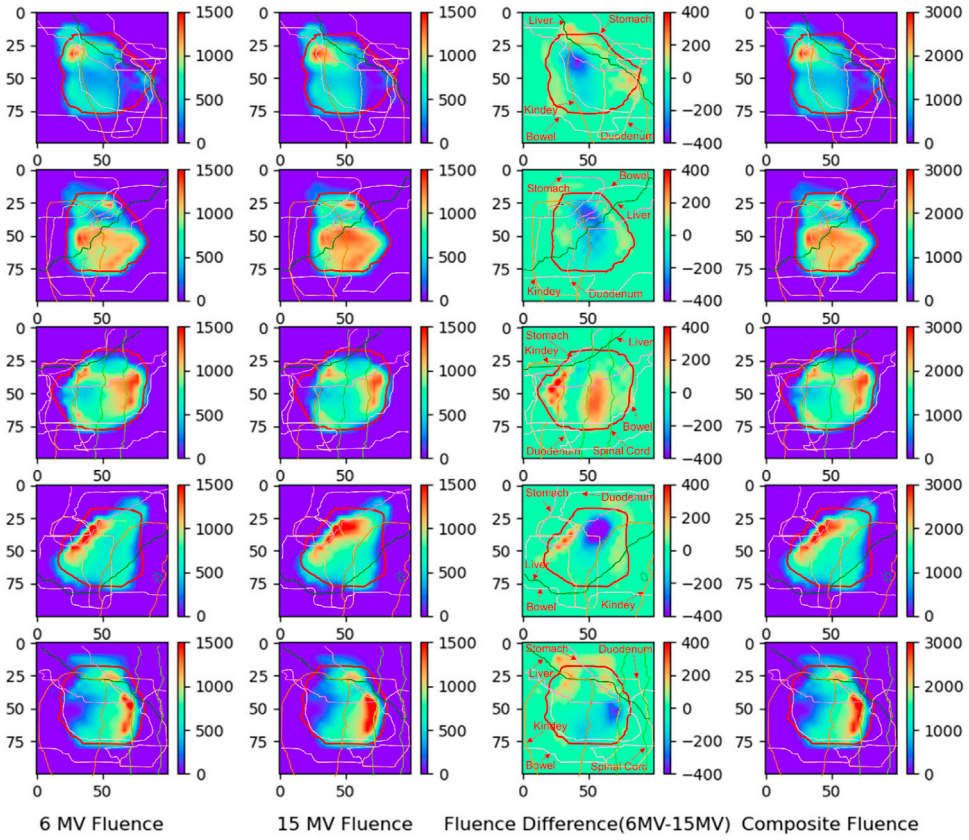

FIGURE 5
The fluence map distributions of the IMRT-BEM plan for one case (from top to down was field 1–5 at the angle of 210°, 300°, 0°, 60°, and 150°, respectively). The thick red outline in the figure is PTV.

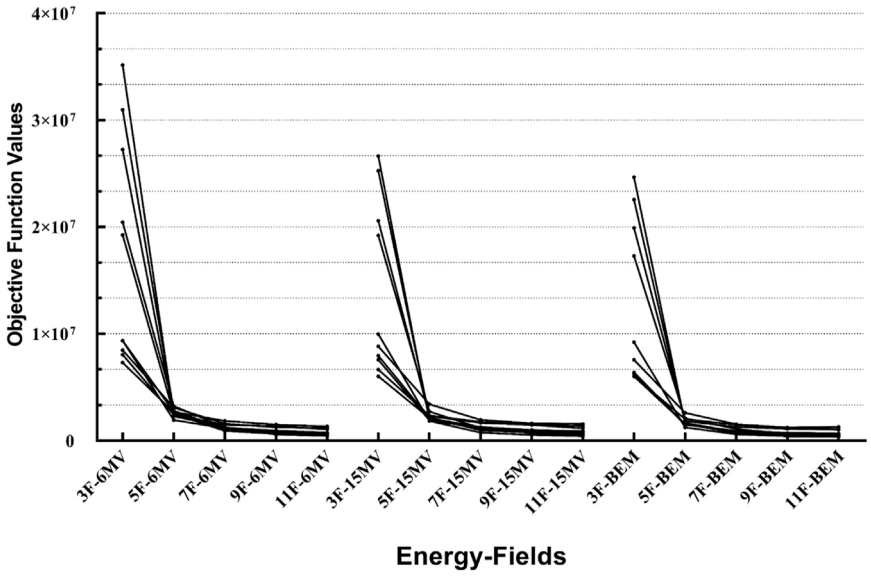

FIGURE 6
The effect of beam energy under different numbers of fields.

Exploring the benefits of lower energy photons opens up new possibilities in radiation therapy planning and treatment. However, it is important to thoroughly evaluate the specific requirements of individual cases and consider factors such as tumor depth, target volume, and surrounding critical structures when determining the optimal photon energy for treatment. Consequently, in future research, the IMRT-BEM algorithm can use energies lower than 6 MV, such as 2 MV, to continue exploring the advantages of low-energy photon beams in radiotherapy. However, it is important to acknowledge that there are also some drawbacks associated with low-energy beams. These include a lower output dose rate, limited maximum dose depth, and reduced penetration capabilities. Additionally, careful planning is required when using low-energy photons to avoid higher dose deposition in the tissue at the entrance of the beam.

In conventional practice, the optimal beam energy is often selected according to the effective path length at a given gantry angle through the body, assigning higher energy to beams with longer path lengths [21]. Although this processing method seems intuitive, it ignores the dose accumulation effect of multiple radiation beams and the complex three-dimensional dosimetric distribution [25]. It was proved that the mixed energy technique is a practical way to generate a homogenous dose distribution for the target or reduce the dose to the OARs while maintaining adequate target coverage. A hybrid photon energy technology is only a simple linear combination of two energy photon plans, which is commonly used for breast and prostate cancers [21, 37, 38]. Obviously, The results obtained by this method are not optimal, and the arbitrariness of the photon energy of a beam increases the possibility of optimization to obtain a suboptimal plan [39]. The optimal and possibly unintuitive plan can be found through energy modulation in inverse planning. However, limited by computing power and system memory, all these studies only selected two photon energies for IMRT optimization research and failed to explore the continuous modulation of photon energy as we did [24, 25]. Besides, their methods all were verified on a small number of clinical cases or ideal water phantom data with the conclusion lacking sufficient clinical statistical data support.

It is a new way to realize energy-modulated IMRT based on two levels of energy photon on a medical linear accelerator with conventional configuration. In theory, compared to conventional single-energy IMRT plans, a beam in IMRT-BEM plans is composed of multiple small sub-beams with different photon energies, allowing separate optimization of different beamlet energies for different parts of the target volume. This may lead to clinical dosimetric improvements in some complex cases with off-center targets or concave tumors adjacent to many OARs of serial or parallel tissue. In this work, we pioneered the application of the concept of continuous photon energy modulation in IMRT planning and showed some advantages of the proposed method. In the future, we will study other tumor sites to identify the scenarios where this method is more useful. The results of this study show that the IMRT-BEM could improve the CI and HI of the plan, and provided a significant reduction of high-dose irradiation volume of the PTV($PTV_{105\%}$), at least 24.7%. Compared with the single-energy IMRT plan (IMRT-6MV or IMRT-15MV), the irradiation volumes of the medium dose (V_{20Gy} and V_{40Gy}) to the duodenum and V_{20Gy} of the stomach were reduced significantly than the other solutions, which may decrease the late toxicity of the duodenum. Research has shown that radiation dose escalation for pancreatic cancer is limited by the proximity of the sensitive surrounding OARs, in particular, gastrointestinal organs which are directly adjacent to the pancreas [40]. Therefore, the reduction of the bowel and the duodenum dose may help to further escalate the dose of PTV in IMRT-BEM, which requires further research to verify.

Though the advantage of the IMRT-BEM plan over the 15 MV plan may not be as pronounced as that over the IMRT-6MV plan, it is important to note that even modest improvements resulting from energy modulation contribute to the development of a more favorable treatment plan. Besides, our study also indicates that, in comparison to the IMRT-15MV plan, the IMRT-BEM plan exhibits a significantly lower monitor unit (MU) value contributed by the 15 MV photon, which reduces the neutron generated.

The focus of this study is to evaluate the effect of beamlet energy modulation. To exclude the dosimetric effect of other factors, the same optimization objectives and constraints were used across all plans for each patient. However, in radiotherapy practice, the optimization goals and constraints can be appropriately adjusted during the optimization to meet the individual dose-volume constraints of different cases. Therefore, the plan quality of IMRT-BEM may be further improved.

In this study, five beams were used. One may ask whether the dosimetric advantages of the IMRT-BEM technique still be valid when the number of beams increases. Therefore, some additional explorations were done in this regard. We found that IMRT-BEM can obtain the lowest objective value when the number of beams is less than 9, as shown in Figure 6. When the number of beams increased, the objective function values of different plans are close to the same, consistent with previous research [15]. Therefore, for some complex cases, we can reduce the dependence of the plan on energy by increasing the number of beams. In radiotherapy practice, the number of beams is generally selected to be 5-7, and the IMRT-BEM technology could be used to deal with some complex cases.

The findings of this study illustrate the different contributions of photons with varying energies to the fluence intensity of the IMRT-BEM plan. Although the synthesized beams cannot perfectly replicate real beams with identical energy levels, they do exhibit dose equivalence in terms of measurable dose effects. Nevertheless, disparities exist in their energy spectral distributions. For instance, a real 10 MV photon beam possesses a maximum photon energy of 10 MeV, whereas a synthesized 10 MV beam has a maximum photon energy equivalent to the highest energy photon employed during synthesis, which could be 15 MeV or 18 MeV. However, when comparing two treatment plans utilizing photons with different energies within the clinically utilized energy range, the primary emphasis lies on their respective doses rather than disparities in beam spectra and energies. However, the differences in other beam modification devices were not taken into consideration in energy modulation, such as leaf transmission and dosimetric leaf gap, which are photon energy dependent. However, they are monotonically changing with energy, these negligible differences may not be observed in our plan comparisons due to the "interpolation" nature of the energy synthesis.

After the optimization of IMRT-BEM, the fluence map of continuous photon energy in each beam was converted into two separate fluence maps corresponding to the low and high photon energies. Then, using a subfield segmentation algorithm, the fluence of each energy was divided into multiple dynamic subfield sequences. Each beam defines two sets of MLC shapes and their respective weights (MUs) for high and low energy, respectively. Ultimately, the IMRT-BEM plan is transformed into two

single-energy photon plans, one with energy E_{low} and the other with energy E_{high}, for delivery. This approach, which utilizes a continuous photon energy modulation optimization strategy, effectively increases the total number of beamlets only by a factor of two in all beam directions, without significantly adding complexity to IMRT optimization and calculation processes. Thus, the algorithm can be efficiently implemented. As for MLC sequencing itself, the sequencing for 6 MV and 15 MV photon beams does not differ from that for single energy beams and can be performed using existing algorithms.

For the IMRT-BEM plan, each beam needs to be converted to two MLC sequences with 6 MV and 15 MV photon beams respectively with two possible delivery strategies. One strategy is to deliver all beams at one energy first and then the other energy. In this case, only one energy switch needs to be performed but the gantry rotation time (field switch time) is doubled. The other strategy is to deliver the beam angle by angle, which involves as much energy switch as the number of beams. The delivery strategy can be chosen by the characteristics of the linac. For Linac with the ability of quick energy switch, ex. less than 20 s on a Varian TrueBeam linac, the second delivery strategy would be preferred.

Certainly, there are shortcomings in this optimization method. One obvious limitation is the extended treatment time caused by the requirement for delivery at two photon energies and increased plan MUs compared with single energy plans (Figure 3). However, this may not be a serious issue because the delivery time is taking less portion of the time slot compared with other steps such as patient setup and image guidance, and the continued development in the linac delivery automation will improve the efficiency of IMRT-BEM. Another limitation is 15 MV photon was used in the IMRT-BEM and neutrons will be produced which may lead to an increased incidence of secondary cancers after photon radiotherapy [35]. However, recent studies have shown that the high-energy neutron component may have been overestimated in the past [41]. More studies are needed to evaluate the effect of using the 15 MV photon beam in radiotherapy.

5 Conclusion

We developed a novel optimization algorithm to include continuous photon beamlet energy modulation in IMRT through the use of photon energy synthesis and validated it in pancreatic cancers. The dosimetric properties of both PTV and some OARs are superior to single-energy IMRT plans. The integral dose of IMRT-BEM is lower than that of IMRT-6MV but slightly higher than IMRT-15MV. The preliminary results demonstrate that the IMRT-BEM algorithm can improve plan quality, especially for complex cases with off-center and concave tumors adjacent to many OARs of serial or parallel tissue.

Data availability statement

The original contributions presented in the study are included in the article/Supplementary Material, further inquiries can be directed to the corresponding authors.

Ethics statement

The studies involving humans were approved by Peking University Third Hospital Medical Science Research Ethics Committee. The studies were conducted in accordance with the local legislation and institutional requirements. Written informed consent for participation was not required from the participants or the participants' legal guardians/next of kin in accordance with the national legislation and institutional requirements.

Author contributions

XZ organized and performed experiments design, data collection, curation, data analysis, and interpretation. He was responsible for writing and revising the manuscript. FZ participated in the study design. BL initiated the project and participated in the study design, and revising of the manuscript. TX collated some experimental data. XB participated in part of the research design. QW initiated the project and participated in the study design, interpretation, and revising of the manuscript. All authors contributed to the article and approved the submitted version.

Funding

This work was supported by the National Key Research and Development Program of China (Nos 2018YFA0704100 and 2018YFA0704101), the Beijing Natural Science Foundation (Nos L222034, L222104 and 7232340), the National Natural Science Foundation of China (No. 61971443) and the Fundamental Research Funds for the Central Universities.

Conflict of interest

The authors declare that the research was conducted in the absence of any commercial or financial relationships that could be construed as a potential conflict of interest.

Publisher's note

All claims expressed in this article are solely those of the authors and do not necessarily represent those of their affiliated organizations, or those of the publisher, the editors and the reviewers. Any product that may be evaluated in this article, or claim that may be made by its manufacturer, is not guaranteed or endorsed by the publisher.

Supplementary material

The Supplementary Material for this article can be found online at: https://www.frontiersin.org/articles/10.3389/fphy.2023.1205650/full#supplementary-material

References

1. Brahme A, Roos JE, Lax I. Solution of an integral equation encountered in rotation therapy. *Phys Med Biol* (1982) 27:1221–9. doi:10.1088/0031-9155/27/10/002

2. Webb S. The physical basis of IMRT and inverse planning. *Br J Radiol* (2003) 76: 678–89. doi:10.1259/bjr/65676879

3. Schreibmann E, Xing L. Feasibility study of beam orientation class-solutions for prostate imrt. *Med Phys* (2004) 31:2863–70. doi:10.1118/1.1797571

4. Shepard DM, Ferris MC, Olivera GH, Mackie TR. Optimizing the delivery of radiation therapy to cancer patients. *Siam Rev Soc Ind Appl Math* (1999) 41:721–44. doi:10.1137/s0036144598342032

5. Kamath S, Sahni S, Li J, Palta J, Ranka S. Leaf sequencing algorithms for segmented multileaf collimation. *Phys Med Biol* (2003) 48:307–24. doi:10.1088/0031-9155/48/3/303

6. Potrebko PS, Fiege J, Biagioli M, Poleszczuk J. Investigating multi-objective fluence and beam orientation IMRT optimization. *Phys Med Biol* (2017) 62:5228–44. doi:10.1088/1361-6560/aa7298

7. Wu Q, Djajaputra D, Lauterbach M, Wu Y, Mohan R. A fast dose calculation method based on table lookup for IMRT optimization. *Phys Med Biol* (2003) 48: N159–66. doi:10.1088/0031-9155/48/12/401

8. Aubry JF, Beaulieu F, Sevigny C, Beaulieu L, Tremblay D. Multiobjective optimization with a modified simulated annealing algorithm for external beam radiotherapy treatment planning. *Med Phys* (2006) 33:4718–29. doi:10.1118/1.2390550

9. Webb S, Convery DJ, Evans PM. Inverse planning with constraints to generate smoothed intensity-modulated beams. *Phys Med Biol* (1998) 43:2785–94. doi:10.1088/0031-9155/43/10/008

10. Zhao X, Liu H, Zhang T. A two-point step size gradient method for non-negative matrix factorization. *Comput Phys* (2011) 164–7. doi:10.1109/ICEOE.2011.6013452

11. Shepard DM, Earl MA, Li XA, Naqvi S, Yu C. Direct aperture optimization: A turnkey solution for step-and-shoot IMRT. *Med Phys* (2002) 29:1007–18. doi:10.1118/1.1477415

12. Bedford JL, Webb S. Constrained segment shapes in direct-aperture optimization for step-and-shoot IMRT. *Med Phys* (2006) 33:944–58. doi:10.1118/1.2163832

13. Stanton R. Dosimetric considerations in the choice of photon energy for external beam radiation therapy: clinical examples. *Med Dosim* (1991) 16:213–9. doi:10.1016/0958-3947(91)90085-g

14. Laughlin JS, Mohan R, Kutcher GJ. Choice of optimum megavoltage for accelerators for photon beam treatment. *Int J Radiat Oncol* (1986) 12:1551–7. doi:10.1016/0360-3016(86)90277-4

15. Pirzkall A, Carol MP, Pickett B, Xia P, Roach MR, Verhey LJ. The effect of beam energy and number of fields on photon-based IMRT for deep-seated targets. *Int J Radiat Oncol Biol Phys* (2002) 53:434–42. doi:10.1016/S0360-3016(02)02750-5

16. Soderstrom S, Eklof A, Brahme A. Aspects on the optimal photon beam energy for radiation therapy. *Acta Oncol* (1999) 38:179–87. doi:10.1080/028418699431591

17. de Boer SF, Kumek Y, Jaggernauth W, Podgorsak MB. The effect of beam energy on the quality of IMRT plans for prostate conformal radiotherapy. *Technol Cancer Res Treat* (2007) 6:139–46. doi:10.1177/153303460700600211

18. Tyagi A, Supe SS, SandeepSingh MP. A dosimetric analysis of 6 mv versus 15 mv photon energy plans for intensity modulated radiation therapy (IMRT) of carcinoma of cervix. *Rep Pract Oncol Radiother* (2010) 15:125–31. doi:10.1016/j.rpor.2010.08.002

19. Wei Z, Peng X, He L, Wang J, Liu Z, Xiao J. Treatment plan comparison of volumetric-modulated arc therapy to intensity-modulated radiotherapy in lung stereotactic body radiotherapy using either 6- or 10-mv photon energies. *J Appl Clin Med Phys* (2022) 23:e13714. doi:10.1002/acm2.13714

20. Henry J, Moreno C, Crownover RL, Baacke D, Papanikolaou N, Gutierrez AN. Dosimetric quantification of dose fall-off in liver SBRT planning using dual photon energy IMRT. *J Radiosurg Sbrt* (2016) 4:145–51.

21. Park JM, Choi CH, Ha SW, Ye S. The dosimetric effect of mixed-energy IMRT plans for prostate cancer. *J Appl Clin Med Phys* (2011) 12:147–57. doi:10.1120/jacmp.v12i4.3563

22. Abdul HK, Shakir KK, Siddhartha A, Siji CT, Musthafa MM, Ganapthi RR. Dosimetric studies of mixed energy intensity modulated radiation therapy for prostate cancer treatments. *J Radiother* (2014) 2014:1–7. doi:10.1155/2014/760206

23. Zhang Y, Feng Y, Ming X, Deng J. Energy modulated photon radiotherapy: A Monte Carlo feasibility study. *Biomed Res Int* (2016) 2016:1–16. doi:10.1155/2016/7319843

24. St-Hilaire J, Sevigny C, Beaulieu F, Gingras L, Tremblay D, Beaulieu L. Optimization of photon beam energy in aperture-based inverse planning. *J Appl Clin Med Phys* (2009) 10:36–54. doi:10.1120/jacmp.v10i4.3012

25. McGeachy P, Villarreal-Barajas JE, Zinchenko Y, Khan R. Modulated photon radiotherapy (XMRT): an algorithm for the simultaneous optimization of photon beamlet energy and intensity in external beam radiotherapy (EBRT) planning. *Phys Med Biol* (2016) 61:1476–98. doi:10.1088/0031-9155/61/4/1476

26. Wu QW, Addido J, Zhuang T, Zhou S. Synthetic photon energy on linac for radiation therapy. *Med Phys* (2017) 44:3305.

27. Zhang X, Zhou F, Liu B, Xiong T, Bai X, Wu Q. Does radiation therapy need more than two photon energies from linac? *Front Oncol* (2022) 12:1009553. doi:10.3389/fonc.2022.1009553

28. Zarepisheh M, Hong L, Zhou Y, Huang Q, Yang J, Jhanwar G, et al. Automated and clinically optimal treatment planning for cancer radiotherapy. *Informs J Appl Anal* (2022) 52:69–89. doi:10.1287/inte.2021.1095

29. Mori S, Hara R, Yanagi T, Sharp GC, Kumagai M, Asakura H, et al. Four-dimensional measurement of intrafractional respiratory motion of pancreatic tumors using a 256 multi-slice ct scanner. *Radiother Oncol* (2009) 92:231–7. doi:10.1016/j.radonc.2008.12.015

30. Ding X, Dionisi F, Tang S, Ingram M, Hung CY, Prionas E, et al. A comprehensive dosimetric study of pancreatic cancer treatment using three-dimensional conformal radiation therapy (3DCRT), intensity-modulated radiation therapy (IMRT), volumetric-modulated radiation therapy (VMAT), and passive-scattering and modulated-scanning proton therapy (pt). *Med Dosim* (2014) 39:139–45. doi:10.1016/j.meddos.2013.11.005

31. Aoyama H, Westerly DC, Mackie TR, Olivera GH, Bentzen SM, Patel RR, et al. Integral radiation dose to normal structures with conformal external beam radiation. *Int J Radiat Oncol Biol Phys* (2006) 64:962–7. doi:10.1016/j.ijrobp.2005.11.005

32. Florence H, Karyn AG, David A, Severine R, Ross AA. Radiotherapy technical considerations in the management of locally advanced pancreatic cancer: american-French consensus recommendations. *Int J Radiat Oncol Biol Phys* (2012) 83.

33. Gregoire V, Mackie TR, De Neve W, Gospodarowicz M, Purdy JA, van Herk M, et al. Icru report 83: prescribing, recording, and reporting photon-beam intensity-modulated radiation therapy (IMRT). *ICRU* (2010) 10:1–106. doi:10.1007/s00066-011-0015-x

34. Das IJ, Kase KR. Higher energy: is it necessary, is it worth the cost for radiation oncology? *Med Phys* (1992) 19:917–25. doi:10.1118/1.596779

35. Kry SF, Salehpour M, Followill DS, Stovall M, Kuban DA, White RA, et al. The calculated risk of fatal secondary malignancies from intensity-modulated radiation therapy. *Int J Radiat Oncol Biol Phys* (2005) 62:1195–203. doi:10.1016/j.ijrobp.2005.03.053

36. Keller BM, Beachey DJ, Pignol JP. Experimental measurement of radiological penumbra associated with intermediate energy x-rays (1 mv) and small radiosurgery field sizes. *Med Phys* (2007) 34:3996–4002. doi:10.1118/1.2775666

37. Birgani MT, Fatahiasl J, Hosseini SM, Bagheri A, Behrooz MA, Zabiehzadeh M, et al. Breast radiotherapy with mixed energy photons; A model for optimal beam weighting. *Asian Pac J Cancer Prev* (2015) 16:7785–8. doi:10.7314/apjcp.2015.16.17.7785

38. Pokharel S. Dosimetric impact of mixed-energy volumetric modulated arc therapy plans for high-risk prostate cancer. *Int J Cancer Ther Oncol* (2013) 1:1011. doi:10.14319/ijcto.0101.1

39. Huang Y, Li S, Yue H, Wang M, Hu Q, Wang H, et al. Impact of nominal photon energies on normal tissue sparing in knowledge-based radiotherapy treatment planning for rectal cancer patients. *Plos One* (2019) 14:e0213271. doi:10.1371/journal.pone.0213271

40. Rao AD, Feng Z, Shin EJ, He J, Waters KM, Coquia S, et al. A novel absorbable radiopaque hydrogel spacer to separate the head of the pancreas and duodenum in radiation therapy for pancreatic cancer. *Int J Radiat Oncol Biol Phys* (2017) 99:1111–20. doi:10.1016/j.ijrobp.2017.08.006

41. Cosset JM, Nassef M, Saidi R, Pugnaire J, Ben AA, Noel A. Which photon energy for intensity-modulated radiotherapy and volumetric-modulated arctherapy in 2019? *Cancer Radiother* (2019) 23:58–61. doi:10.1016/j.canrad.2018.04.003